

# Bound on resistivity in flat band materials due to the quantum metric

Johannes Mitscherling<sup>1</sup> and Tobias Holder<sup>2</sup>

<sup>1</sup>Max Planck Institute for Solid State Research, Heisenbergstrasse 1, 70569, Stuttgart, Germany

<sup>2</sup>Department of Condensed Matter Physics, Weizmann Institute of Science, Rehovot, Israel 76100

(Dated: March 22, 2022)

The quantum metric is a central quantity of band theory but has so far not been related to many response coefficients due to its non-classical origin. However, within a newly developed Kubo formalism for fast relaxation, the decomposition of the dc electrical conductivity into both classical (intraband) and quantum (interband) contributions recently revealed that the interband part is proportional to the quantum metric. Here, we show that interband effects due to the quantum metric can be significantly enhanced and even dominate the conductivity for semimetals at charge neutrality and for systems with highly quenched bandwidth. This is true in particular for topological flat band materials of nonzero Chern number, where an upper bound exists for the resistivity due to the common geometrical origin of quantum metric and Berry curvature. We suggest to search for these effects in highly tunable rhombohedral trilayer graphene flakes.

## I. INTRODUCTION

Recent experimental progress has made it possible to investigate new two-dimensional quantum materials with a highly quenched bandwidth, which exhibit a rich phase diagram including unconventional superconducting phases, correlated insulating states and a cascade of magnetic and non-magnetic flavor-ordered states [1–14]. While the most interesting phenomena in the ordered states are due to many-body effects, these findings have also ignited renewed interest in understanding the normal state of moiré-type and periodic lattice systems with vanishing Fermi velocity [15–18]. However, remarkably little is known about the effects of a quenched bandwidth on the electrical conductivity. In this work, we systematically investigate the interplay between band structure and conductivity using a non-interacting Kubo approach which allows to fully identify and quantify the various contributing factors.

The two paradigmatic flat band systems are twisted bilayer graphene (TBG), a van-der-Waals material where the second layer is put askew by a small angle [19,20]; and rhombohedral trilayer graphene (RTG), where three graphene monolayers are layered on top of each other without twist, with atomic positions in the sequence A-B-C [21–24]. Here, we will only discuss the latter material, because with the availability of high mobility samples, it offers a viable platform to study band structure effects. On the theoretical side, the implications of a highly quenched band width challenge the existing theories as, for instance, the superfluid stiffness should vanish in the limit of flat bands, which would forbid a superconducting state at finite temperature [25]. In this context, several indications have been found that a quantity known as the quantum metric provides the relevant contribution to the superfluid stiffness of the superconducting state [26–29]. The quantum metric has previously been connected to the size of a maximally localized Wannier state [30,31] and is crucial in the modern theory of polarization [32]. Only recently, its importance was noticed in other contexts [33–37].

The quantum metric is a central quantity of band theory, comparable to the Berry curvature. Both can be combined into the quantum geometric tensor, which captures important geometrical properties of the manifold that is formed by the Bloch eigenstates [38]. At the same time, due to its non-classical origin the quantum metric could not be related to many response coefficients. For example, the quantum metric has not been measured neither in the superconducting nor in the normal state of both TBG and RTG.

Recently, a new formulation of the Kubo formalism in two-band models for arbitrary band broadening  $\Gamma$  (i.e. fast quasiparticle relaxation rate) was developed by one of us and revealed that the static charge conductivity *does* contain an interband contribution proportional to the quantum metric [39]. However in a metallic state, the interband term is generically of order  $\sim \Gamma$ , so that it is strongly suppressed compared to the intraband (Drude-type) response of size  $\sim \Gamma^{-1}$  in the clean limit. The interband effect and its sensitivity to the relaxation rate can be understood either semiclassically as the overlap of separated bands upon band broadening; or in perturbation theory one would attribute it to virtual excitations across the energy gap [cf. Fig. 1]. In the following, we will establish under which conditions interband effects due to the quantum metric can substantially contribute or even dominate the conductivity.

The key observation is that the scaling argument above is only valid in the metallic state with a Fermi surface, on which the quasiparticle velocities and the quantum metric are approximately constant. This certainly does not apply to semimetals at charge neutrality, where the Fermi surface reduces to a single point in momentum space, at which the quantum metric diverges. In systems with a flat band, the vanishingly small bandwidth results in a very small Drude conductivity compared to the quantum metric contribution. These observations are in line with the interpretation of the quantum metric as a measure of the deformation of the wavepacket as it traverses the lattice [40], such deformations are facilitated by the large size of a wavepacket in real space for semimetals or

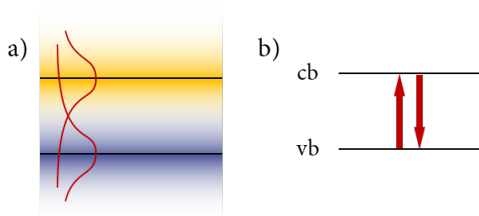


Figure 1. Emergence of the longitudinal interband conductivity for a band structure with a finite broadening  $\Gamma$ . (a) According to semiclassics, there is a finite density of states from the conduction band (cb) present at the valence band (vb), and vice versa, that is introduced by the band broadening in the respective other band. (b) According to perturbation theory the bands are defined sharply; instead a finite carrier lifetime allows virtual processes involving remote bands.

momentum space for flatband systems.

We show that the new Kubo formalism for fast relaxation is capable to treat the different cases within one theory. The formalism is based on a phenomenological quasiparticle relaxation rate  $\Gamma$  of arbitrary size. This regularizes the spectral occupation, which results in smooth conductivity formulas and allow for a systematic expansion in  $\Gamma$ . Since the previous formulation in Ref. [39] was limited to two bands, we present here a self-contained generalization to a general number of bands.

For semimetals at charge neutrality, the divergence of the quantum metric is compensated by a vanishing spectral occupation. For a two-dimensional Dirac cone, we recover the well-known result  $\sigma^{xx} = e^2/\pi h$  [41] independent of  $\Gamma$ . We find that both quantum metric and intraband contribution provide half of this result. For four different models, we find that the intraband and quantum metric contributions are of the same order in  $\Gamma$ .

Flat band systems are particular interesting, since the vanishing quasiparticle velocity drastically reduces the intraband contribution. We therefore expect the quantum metric to prominently enter the dc conductivity in systems with highly quenched bandwidth. To this end, we calculate the normal state conductivity in the flat band limit for a band structure with arbitrary lifetime broadening. As expected, the interband term can become even larger than the Drude term. Additionally, the conductivity develops a plateau for an intermediate regime  $W_{\text{flat}} < \Gamma < \Delta_{\text{gap}}$  of band broadening. Here, the lower limit of the plateau is given by the small bandwidth  $W_{\text{flat}}$  of the quenched band, while the band gap  $\Delta_{\text{gap}}$  to neighboring bands present the upper limit.

The quantum metric  $g$  and the Berry curvature  $\Omega$  are the real and imaginary part of the quantum geometric tensor, respectively, which is positive semi-definite [26]. This imposes a constraint on their components  $g^{\alpha\beta}$  and  $\Omega^{\alpha\beta}$ , which imposes a lower bound  $\int_{\mathbf{p}} \text{tr } g \geq \int_{\mathbf{p}} |\Omega^{xy}| \geq C/2\pi$  in two-dimensional systems [26,42,43], where  $C$  is the Chern number. Based on the interpretation of the quantum metric as spread of the wave functions, this prop-

erty is also known as "Wannier obstruction" [30,31,44]. In two-dimensional flat band systems in the regime  $W_{\text{flat}} < \Gamma < \Delta_{\text{gap}}$  of band broadening, we find that the trace over the quantum metric contribution is proportional to  $\int_{\mathbf{p}} \text{tr } g$  and, thus, bounded from below. This implies a new upper bound on the resistivity, which is unrelated to previous bounds which were suggested due to strong interactions and the related fast thermalization of quasiparticles [16,45–47]. We reemphasize that the bound is not a universal limit, because it only holds within a certain regime of relaxation rates.

We propose to use low-mobility RTG samples as a platform to search for the quantum metric effect experimentally. In particular, we suggest to study the temperature dependence of the conductivity and predict a conductivity minimum below room temperature as a result of decreasing classical (intraband) and increasing quantum metric (interband) contributions. In RTG both intraband and interband contributions are of similar size over the full temperature range in contrast to perfect flat band systems, where the energy scales are well separated. Nevertheless, we can clearly assign the conductivity minimum at the predicted temperatures to the quantum metric, since a conductivity upturn due to thermal activation of higher bands take place far beyond room temperature. We find the minimum for a broad range of tunable parameters.

The paper is structured as follows: We present the Kubo formalism for fast relaxation for a general multi-band system and present our key formulas for the conductivity. The role of band broadening is discussed for metals, semimetals, and flat bands, where the bound on the resistivity is derived. The theory is then applied to a generic flat band model and RTG. We summarize our findings in the conclusions.

## II. RESULTS

### A. Conductivity formulas

We consider a non-interacting quadratic tight-binding Hamiltonian for an  $N$ -band system

$$H = \sum_{\mathbf{p}} \Psi_{\mathbf{p}}^{\dagger} \lambda_{\mathbf{p}} \Psi_{\mathbf{p}}, \quad (1)$$

where the spinor  $\Psi_{\mathbf{p}} = (c_{\mathbf{p},1}, \dots, c_{\mathbf{p},N})$  and its complex conjugate  $\Psi_{\mathbf{p}}^{\dagger}$  involve the fermionic annihilation and creation operators of the  $N$  bands at (crystal) momentum  $\mathbf{p}$ , respectively.  $\lambda_{\mathbf{p}}$  is the Hermitian  $N \times N$  Bloch Hamiltonian matrix.

We calculate the dc conductivity given by

$$\sigma^{\alpha\beta} = - \lim_{\omega \rightarrow 0} \frac{1}{i\omega} \Pi^{\alpha\beta}(\omega), \quad (2)$$

where  $\alpha$  and  $\beta$  denote the spatial directions of the current and the electric field, respectively, in  $d$  dimensions. The following derivation generalizes the approach developed

by one of us from two to  $N$  bands [39]. The polarization tensor  $\Pi^{\alpha\beta}(\omega)$  is obtained by the Kubo formula

$$\Pi_{iq_0}^{\alpha\beta} = \frac{e^2 k_B T}{\hbar V} \sum_{ip_0, \mathbf{p}} \text{tr} [\mathcal{G}_{ip_0+iq_0, \mathbf{p}} \lambda_{\mathbf{p}}^{\beta} \mathcal{G}_{ip_0, \mathbf{p}} \lambda_{\mathbf{p}}^{\alpha} - (iq_0 = 0)] \quad (3)$$

after analytic continuation of the bosonic Matsubara frequency  $iq_0 \rightarrow \omega + i0^+$  to real frequency  $\omega$ . The polarization tensor (3) involves the generalized velocities, that is, the momentum derivatives of the Bloch matrix in Eq. (1),  $\lambda_{\mathbf{p}}^{\alpha} = \partial_{\alpha} \lambda_{\mathbf{p}}$ , and the Green's function matrix

$$\mathcal{G}_{ip_0, \mathbf{p}} = [ip_0 + \mu - \lambda_{\mathbf{p}} + i\Gamma \text{sign}(p_0)]^{-1} \quad (4)$$

with fermionic Matsubara frequency  $ip_0$ . We denote the trace over the  $N$  bands as  $\text{tr}$ .  $T$  is the temperature and  $V$  the volume of the Brillouin zone. The second term in Eq. (3) is the diamagnetic term, which is equal to the first term with  $iq_0$  set to zero.

The key in the used approach is to consider a phenomenological relaxation rate  $\Gamma > 0$ , which is not restricted in size in the following derivation [39]. For simplicity,  $\Gamma$  is assumed to be frequency- and momentum-independent as well as equal for all bands.

We diagonalize the Bloch Hamiltonian  $\lambda_{\mathbf{p}}$  by its  $N$  eigenvectors  $|n_{\mathbf{p}}\rangle$  with corresponding eigenvalues  $E_{\mathbf{p}}^n$ . The elements of the Green's function and the generalized velocities in the eigenbasis then read

$$\mathcal{G}_{ip_0, \mathbf{p}}^n = [ip_0 + \mu - E_{\mathbf{p}}^n + i\Gamma \text{sign}(p_0)]^{-1}, \quad (5)$$

$$(\tilde{\lambda}_{\mathbf{p}}^{\alpha})_{nm} = \delta_{nm} v_{\mathbf{p}}^{\alpha, n} + i(E_{\mathbf{p}}^n - E_{\mathbf{p}}^m) \mathcal{A}_{\mathbf{p}}^{\alpha, nm}, \quad (6)$$

where we denote the quasiparticle velocities as  $v_{\mathbf{p}}^{\alpha, n} = \partial_{\alpha} E_{\mathbf{p}}^n$  and the Berry connection as  $\mathcal{A}_{\mathbf{p}}^{\alpha, nm} = i\langle n_{\mathbf{p}} | \partial_{\alpha} m_{\mathbf{p}} \rangle$ .  $\delta_{nm}$  is the Kronecker delta. Note that the quasiparticle Green's function (5) is diagonal, whereas the generalized velocity (6) has both diagonal and off-diagonal contributions leading to both intraband and interband contributions to the conductivity tensor  $\sigma^{\alpha\beta}$ . Furthermore, we uniquely decompose  $\sigma^{\alpha\beta}$  into its symmetric and antisymmetric parts under the exchange of  $\alpha \leftrightarrow \beta$ . After performing the Matsubara summation, analytic continuation, and the thermodynamic limit  $1/V \sum_{\mathbf{p}} \rightarrow \int d^d \mathbf{p} / (2\pi)^d$  we obtain the decomposition

$$\sigma^{\alpha\beta} = \sigma_{\text{intra}}^{\alpha\beta} + \sigma_{\text{inter}}^{\alpha\beta, s} + \sigma_{\text{inter}}^{\alpha\beta, a}. \quad (7)$$

The intraband contribution  $\sigma_{\text{intra}}^{\alpha\beta} = \sigma_{\text{intra}}^{\beta\alpha}$  is symmetric, whereas the interband contribution has both a symmetric part  $\sigma_{\text{inter}}^{\alpha\beta, s} = \sigma_{\text{inter}}^{\beta\alpha, s}$  and an antisymmetric part  $\sigma_{\text{inter}}^{\alpha\beta, a} =$

$-\sigma_{\text{inter}}^{\beta\alpha, a}$ . The three contributions read

$$\sigma_{\text{intra}}^{\alpha\beta} = -\frac{e^2}{\hbar} \int \frac{d^d \mathbf{p}}{(2\pi)^d} \int d\epsilon f'(\epsilon) \sum_n w_{\mathbf{p}, \text{intra}}^n(\epsilon) v_{\mathbf{p}}^{\alpha, n} v_{\mathbf{p}}^{\beta, n}, \quad (8)$$

$$\sigma_{\text{inter}}^{\alpha\beta, s} = -\frac{e^2}{\hbar} \int \frac{d^d \mathbf{p}}{(2\pi)^d} \int d\epsilon f'(\epsilon) \sum_{n, m} w_{\mathbf{p}, \text{inter}}^{nm, s}(\epsilon) g_{\mathbf{p}}^{\alpha\beta, nm}, \quad (9)$$

$$\sigma_{\text{inter}}^{\alpha\beta, a} = -\frac{e^2}{\hbar} \int \frac{d^d \mathbf{p}}{(2\pi)^d} \int d\epsilon f(\epsilon) \sum_{n, m} w_{\mathbf{p}, \text{inter}}^{nm, a}(\epsilon) \Omega_{\mathbf{p}}^{\alpha\beta, nm}, \quad (10)$$

where  $f(\epsilon) = [\exp(\epsilon/k_B T) + 1]^{-1}$  and  $f'(\epsilon)$  are the Fermi distribution and its derivative, respectively. The momentum integration is performed over the  $d$ -dimensional Brillouin zone. We discuss the different quantities in the following. The intraband contribution (8) involves a summation over all bands with their respective quasiparticle velocities  $v_{\mathbf{p}}^{\alpha, n}$ . The two interband contributions (9) and (10) involve a summation over all pairs of bands with

$$g_{\mathbf{p}}^{\alpha\beta, nm} = \text{Re}[\mathcal{A}_{\mathbf{p}}^{\alpha, nm} \mathcal{A}_{\mathbf{p}}^{\beta, mn}], \quad (11)$$

$$\Omega_{\mathbf{p}}^{\alpha\beta, nm} = -2 \text{Im}[\mathcal{A}_{\mathbf{p}}^{\alpha, nm} \mathcal{A}_{\mathbf{p}}^{\beta, mn}], \quad (12)$$

which are invariant under the  $U(1)$  gauge freedom  $|n_{\mathbf{p}}\rangle \rightarrow e^{i\phi_{\mathbf{p}}} |n_{\mathbf{p}}\rangle$  for  $n \neq m$  due to the particular combination of the Berry connections. The summation  $\sum_{n \neq m} \mathcal{A}_{\mathbf{p}}^{\alpha, nm} \mathcal{A}_{\mathbf{p}}^{\beta, mn}$  yields the quantum geometric tensor  $\mathcal{T}_{\mathbf{p}}^{\alpha\beta, n}$ , which decomposes into the symmetric real part  $g_{\mathbf{p}}^{\alpha\beta, n}$  and antisymmetric imaginary part  $-\Omega_{\mathbf{p}}^{\alpha\beta, n}/2$ , that is, the quantum (or Fubini-Study) metric and the Berry curvature, respectively [38],

$$\sum_{m \neq n} g_{\mathbf{p}}^{\alpha\beta, nm} = \sum_{m \neq n} g_{\mathbf{p}}^{\alpha\beta, mn} = g_{\mathbf{p}}^{\alpha\beta, n}, \quad (13)$$

$$\sum_{m \neq n} \Omega_{\mathbf{p}}^{\alpha\beta, nm} = -\sum_{m \neq n} \Omega_{\mathbf{p}}^{\alpha\beta, mn} = \Omega_{\mathbf{p}}^{\alpha\beta, n}. \quad (14)$$

We emphasize that the interband contribution can be interpreted as a pure quantum geometrical quantity. For a two-band system, note that (11) and (12) are already the quantum metric and the Berry curvature, respectively. To highlight the geometric interpretation of the interband contributions, we refer to  $\sigma_{\text{inter}}^{\alpha\beta, s}$  and  $\sigma_{\text{inter}}^{\alpha\beta, a}$  as the quantum metric and the Berry curvature contribution, respectively, in the following.

The three contributions to the conductivity (8)-(10) involve three different spectral weighting factors

$$w_{\mathbf{p}, \text{intra}}^n(\epsilon) = \pi (A_{\mathbf{p}}^n(\epsilon))^2, \quad (15)$$

$$w_{\mathbf{p}, \text{inter}}^{nm, s}(\epsilon) = \pi (E_{\mathbf{p}}^n - E_{\mathbf{p}}^m)^2 A_{\mathbf{p}}^n(\epsilon) A_{\mathbf{p}}^m(\epsilon), \quad (16)$$

$$w_{\mathbf{p}, \text{inter}}^{nm, a}(\epsilon) = 2\pi^2 (E_{\mathbf{p}}^n - E_{\mathbf{p}}^m)^2 [A_{\mathbf{p}}^n(\epsilon)]^2 A_{\mathbf{p}}^m(\epsilon), \quad (17)$$

which are particular combinations of the quasiparticle spectral functions

$$A_{\mathbf{p}}^n(\epsilon) = \frac{1}{\pi} \frac{\Gamma}{\Gamma^2 + (\epsilon + \mu - E_{\mathbf{p}}^n)^2}. \quad (18)$$

	$\sigma_{\text{intra}}^{xx}$	$\sigma_{\text{inter}}^{xx,s}$	$\sigma_{\text{intra}}^{yy}$	$\sigma_{\text{inter}}^{yy,s}$	$\sigma_{\text{intra}}^{zz}$	$\sigma_{\text{inter}}^{zz,s}$	$\sigma_{\text{inter}}^{xx,s}/\sigma_{\text{intra}}^{xx}$	$\sigma_{\text{inter}}^{yy,s}/\sigma_{\text{intra}}^{yy}$	$\sigma_{\text{inter}}^{zz,s}/\sigma_{\text{intra}}^{zz}$
$\lambda_{\mathbf{p}}^{(I)}$	$\frac{1}{2} \frac{a}{b} \frac{1}{\pi}$	$\frac{1}{2} \frac{a}{b} \frac{1}{\pi}$	$\frac{1}{2} \frac{b}{a} \frac{1}{\pi}$	$\frac{1}{2} \frac{b}{a} \frac{1}{\pi}$	-	-	1	1	-
$\lambda_{\mathbf{p}}^{(II)}$	$\frac{1}{\pi}$	$\frac{a^2}{a^2+b^2} \frac{1}{\pi}$	$\frac{1}{\pi}$	$\frac{a^2}{a^2+b^2} \frac{1}{\pi}$	-	-	$\frac{a^2}{a^2+b^2}$	$\frac{a^2}{a^2+b^2}$	-
$\lambda_{\mathbf{p}}^{(III)}$	$0.197 \frac{1}{\sqrt{\Gamma}}$	$0.098 \frac{1}{\sqrt{\Gamma}}$	$0.324\sqrt{\Gamma}$	$0.216\sqrt{\Gamma}$	-	-	$\frac{1}{2}$	$\frac{2}{3}$	-
$\lambda_{\mathbf{p}}^{(IV)}$	$\frac{1}{6} \frac{1}{(bc)^2} \frac{1}{\pi}$	$\frac{1}{3} \frac{1}{(bc)^2} \frac{1}{\pi}$	$\frac{1}{6} \frac{1}{(ac)^2} \frac{1}{\pi}$	$\frac{1}{3} \frac{1}{(ac)^2} \frac{1}{\pi}$	$\frac{1}{6} \frac{1}{(ab)^2} \frac{1}{\pi}$	$\frac{1}{3} \frac{1}{(ab)^2} \frac{1}{\pi}$	2	2	2

Table I. The intraband and the quantum metric contribution to the longitudinal conductivity in  $x$  and  $y$  directions for different models of semimetals (19)-(22) at the charge neutrality point  $\mu = 0$ . The intraband and the quantum metric contribution are of the same order in  $\Gamma$  in all cases. However, their ratio is non-universal. The numerical prefactors for  $\lambda_{\mathbf{p}}^{(III)}$  are rounded for simplicity. The conductivities are given in units of  $e^2/h$ .

Note that  $w_{\mathbf{p},\text{inter}}^{nn,s}(\epsilon) = w_{\mathbf{p},\text{inter}}^{nn,s}(\epsilon) = 0$  for the diagonal components.

We close the general derivation by stressing that no assumptions on the size of  $\Gamma$  were made during the calculation, so that the formulas for the conductivity in Eq. (7) and its contributions (8)-(10) are valid for  $\Gamma$  of arbitrary size. However, the results crucially rely on the assumed simple form of the phenomenological relaxation rate  $\Gamma$ . A generalization, for instance, by using a frequency and momentum dependent  $\Gamma(\mathbf{p}, \omega)$  or a band dependent  $\Gamma_{nm}$ , is beyond the scope of this paper. Furthermore,  $\Gamma$  is assumed without any specification of its physical realization, for instance, due to interaction, impurity scattering, or coupling to the environment, and potential vertex corrections are not taken into account in our calculation. The range of validity of our assumptions have, thus, to be checked within the concrete application.

## B. Role of band broadening

We discuss the dependence on the phenomenological relaxation rate  $\Gamma$ , which is captured by the spectral weighting factors (15)-(17). We distinguish three different cases: the clean limit for a metal, charge neutrality points in (higher-order) Dirac semimetals, and flat bands. We note that the scaling behavior for large  $\Gamma$  and the (topological) properties of the Berry curvature contribution  $\sigma_{\text{inter}}^{\alpha\beta,s}$  were already discussed in Ref. [39] and will not be considered further here.

*a. Clean limit for a metal* In the following, we generalize the results for two-band systems given in Refs. [39,48]. We assume a  $d - 1$ -dimensional Fermi surface. If  $\Gamma$  is so small that for given directions  $\alpha, \beta$ , and bands  $n, m$  the quantities  $v_{\mathbf{p}}^{\alpha,n} v_{\mathbf{p}}^{\beta,n}$ ,  $g_{\mathbf{p}}^{\alpha\beta, nm}$ , and  $\Omega_{\mathbf{p}}^{\alpha\beta, nm}$  are almost constant in a momentum range in which the variation of  $E_{\mathbf{p}}^n$  and  $E_{\mathbf{p}}^m$  is of the order of  $\Gamma$ , we can approximate the spectral weighting factors in Eqs. (15)-(17) by Dirac delta functions with a particular leading-order dependence on  $\Gamma$ :  $w_{\mathbf{p},\text{intra}}^n \sim 1/\Gamma$ ,  $w_{\mathbf{p},\text{inter}}^{nm,s} \sim \Gamma$ , and  $w_{\mathbf{p},\text{inter}}^{nm,a} \sim 1$ . After performing the frequency integration and using (13) and (14), we see that the intraband, the quantum metric and the Berry curvature contributions further decompose

into individual band contributions  $\sigma_{\text{intra},n}^{\alpha\beta} \sim v_{\mathbf{p}}^{\alpha,n} v_{\mathbf{p}}^{\beta,n}$ ,  $\sigma_{\text{inter},n}^{\alpha\beta,s} \sim g_{\mathbf{p}}^{\alpha\beta,n}$ , and  $\sigma_{\text{inter},n}^{\alpha\beta,a} \sim \Omega_{\mathbf{p}}^{\alpha\beta,n}$ , respectively, involving the respective quasiparticle velocities, quantum metric, and Berry curvature. Thus, we recover the well-known semiclassical results for the intraband contribution [49] as well as the dissipationless anomalous Hall conductivity due to the Berry curvature [50,51]. The quantum metric contribution of the longitudinal conductivity is suppressed by  $\Gamma^2/(E_{\mathbf{p}}^n - E_{\mathbf{p}}^m)^2$  compared to the intraband contribution. It provides significant contribution only at small direct band gaps, for instance, at the onset of order at quantum critical points [48,52].

*b. Charge neutrality points in Dirac semimetals* We calculate the longitudinal conductivity explicitly for four different models of (higher-order) Dirac semimetals

$$\lambda_{\mathbf{p}}^{(I)} = a p_x \sigma_x + b p_y \sigma_y, \quad (19)$$

$$\lambda_{\mathbf{p}}^{(II)} = \frac{a}{2} (p_y^2 - p_x^2) \sigma_x + a p_x p_y \sigma_y + \frac{b}{2} |\mathbf{p}|^2 \sigma_z, \quad (20)$$

$$\lambda_{\mathbf{p}}^{(III)} = p_x \sigma_x + p_y^2 \sigma_y, \quad (21)$$

$$\lambda_{\mathbf{p}}^{(IV)} = a p_x \sigma_x + b p_y \sigma_y + c p_z \sigma_z, \quad (22)$$

with parameters  $a, b, c > 0$ .  $\sigma_i$  are Pauli matrices. The Hamiltonian (19) and (22) describe two- and three-dimensional Dirac cones. A quadratic band touching and a mixed linear and quadratic band touching in two dimensions are described by (20) and (21), respectively. We fix the chemical potential  $\mu$  to the charge neutrality point, so that the Fermi surface reduces to a single momentum point. The former considerations do not apply since the quantum metric diverges at that momentum. We perform the momentum integration over  $\mathbb{R}^d$  and at zero temperature.

The results are summarized in Table. I. We find that the intraband contribution and the quantum metric contribution are of the same order in  $\Gamma$ . For (19), (20), and (22) the conductivity is independent of  $\Gamma$ . For (21) we find an unconventional scaling of  $1/\sqrt{\Gamma}$  in  $x$  direction and  $\sqrt{\Gamma}$  in  $y$  direction. In all cases, the size of the quantum metric contribution is of the same order as the intraband contribution. For instance, both  $\sigma_{\text{intra}}^{xx}$  and  $\sigma_{\text{inter}}^{xx,s}$  contribute equally to the longitudinal conductivity of a symmetric

two-dimensional Dirac cone (19) with  $a = b$ , where we obtain again  $\sigma^{xx} = e^2/\pi h$  for a Dirac cone. The ratio between the quantum metric and the intraband contribution is, however, non-universal as explicitly shown for (20) with  $\sigma_{\text{inter}}^{xx,s}/\sigma_{\text{intra}}^{xx} = a^2/(a^2 + b^2)$  for arbitrary  $a, b > 0$ .

*c. Flat band geometry* We study the intraband and the quantum metric contribution for a flat band system. For convenience, we relabel the bands such that the zeroth band is the momentum-independent flat band,  $E_{\mathbf{p}}^0 = E_{\text{flat}}$ . We fix the chemical potential at the flat band energy  $\mu = E_{\text{flat}}$ . We assume that the flat band is isolated such that  $\Gamma \ll |E_{\mathbf{p}}^n - E_{\text{flat}}|$  for all bands  $n \neq 0$  and momenta  $\mathbf{p}$ . Note that the following arguments also hold for bands  $E_{\mathbf{p}}^0$  that are flat on the scale of  $\Gamma$ , i.e.  $|\mu - E_{\mathbf{p}}^0| \ll \Gamma$  for all momenta  $\mathbf{p}$ . For simplicity, we consider zero temperature in the following. The spectral weighting factors involving the flat band are

$$w_{\mathbf{p},\text{intra}}^0(0) \approx \frac{1}{\pi\Gamma^2} \quad (23)$$

$$w_{\mathbf{p},\text{inter}}^{0n,s}(0) = w_{\mathbf{p},\text{inter}}^{n0,s}(0) \approx \frac{1}{\pi} \quad (24)$$

for  $n \neq 0$ . The higher-order terms and the other contributions with  $n, m \neq 0$  are of order  $\mathcal{O}(\Gamma^2/(E_{\mathbf{p}}^n - E_{\text{flat}})^2)$  and, thus, suppressed. Using the formula in Eq. (9) we see that the quantum metric contribution is given by the integral of the quantum metric over the Brillouin zone,

$$\sigma_{\text{inter}}^{\alpha\beta,s} = \frac{2}{\pi} \frac{e^2}{\hbar} \int \frac{d^d \mathbf{p}}{(2\pi)^d} g_{\mathbf{p}}^{\alpha\beta,0}. \quad (25)$$

Rewriting the quantum metric as  $g_{\mathbf{p}}^{\alpha\beta,n} = \langle n_{\mathbf{p}} | \hat{r}_{\alpha} \hat{r}_{\beta} | n_{\mathbf{p}} \rangle - \langle n_{\mathbf{p}} | \hat{r}_{\alpha} | n_{\mathbf{p}} \rangle \langle n_{\mathbf{p}} | \hat{r}_{\beta} | n_{\mathbf{p}} \rangle$  with position operator  $\hat{r}_{\alpha} = i\partial_{\alpha}$  we see that  $\sigma_{\text{inter}}^{\alpha\beta,s}$  for a chemical potential inside the flat band is given by the mean spread of the Bloch wave functions of the flat band [30,31,44,53].

We focus on a two-dimensional system in the following, which we assume to lie in the  $x$ - $y$  plane. The trace of the quantum metric is bounded by the absolute value of the Berry curvature [26,43,54], that is,  $g_{\mathbf{p}}^{xx,n} + g_{\mathbf{p}}^{yy,n} \geq |\Omega_{\mathbf{p}}^{xy,n}|$ , since the quantum geometric tensor  $\mathcal{T}_{\mathbf{p}}^{\alpha\beta}$  is positive semi-definite. Thus, the sum of the quantum metric contribution in  $x$  and  $y$  direction is bounded from below, that is,

$$\sigma_{\text{inter}}^{xx,s} + \sigma_{\text{inter}}^{yy,s} \geq \frac{2}{\pi} \frac{e^2}{\hbar} \int \frac{d^d \mathbf{p}}{(2\pi)^d} |\Omega_{\mathbf{p}}^{xy,0}| \geq \frac{2}{\pi} \frac{e^2}{\hbar} |C_0|, \quad (26)$$

where the Chern number is defined by  $C_n = -2\pi \int \frac{d^2 \mathbf{p}}{(2\pi)^2} \Omega_{\mathbf{p}}^{xy,n} \in \mathbb{Z}$ . We see that the quantum metric contribution and, thus, the longitudinal conductivity is always finite for systems with nonzero Berry curvature. In the next section we explore this bound for a topological flat band with nonzero Chern number, where it is particularly prominent.

The intraband contribution (8) involves the quasiparticle velocities, which are identically zero in a perfect

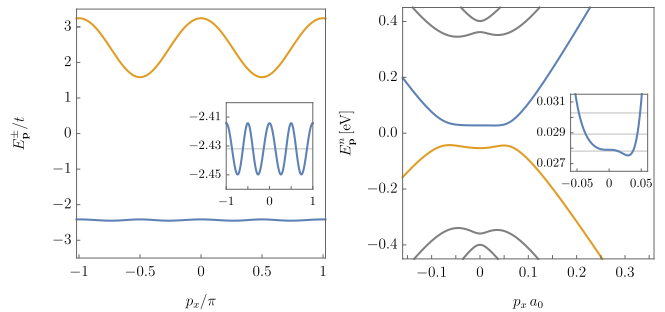


Figure 2. The dispersions of the flat band model (left) and of the model for rhombohedral trilayer graphene (right). The dispersion of the considered flat band (blue) and the chemical potentials are shown in the inset. The band width is much smaller than the gap to the closest band (orange).

flat band. Thus, the conductivity is entirely given quantum metric contribution. In almost flat bands, both intra- and interband processes contribute and it depends on the value of  $\Gamma$  which one is dominant. We can give an estimate on the crossover scale of  $\Gamma$  by setting  $\sigma_{\text{intra}}^{xx} + \sigma_{\text{intra}}^{yy} = \sigma_{\text{inter}}^{xx,s} + \sigma_{\text{inter}}^{yy,s}$ , from which we conclude that the quantum metric related conductivity is dominant for values of the band broadening above a threshold  $\Gamma_c$ , with

$$\Gamma_c \lesssim \sqrt{\frac{\pi}{|C_0|} [(v_{\text{max}}^{x,0})^2 + (v_{\text{max}}^{y,0})^2]} \quad (27)$$

by using (23) and (26) and approximating the quasiparticle velocities by their upper bounds  $v_{\text{max}}^{\alpha,0}$ . However, note that a large estimate for  $\Gamma_c$  does not imply a negligible interband contribution for smaller  $\Gamma$ , as we discuss in a moment using the example of rhombohedral trilayer graphene.

The quantum metric contribution in a flat band systems given by Eq. (25) suggests a pure quantum mechanical mechanism for an anisotropic conductivity based on the underlying wave functions. In particular, an anisotropic quantum metric  $g_{\mathbf{p}}^{xx,0} \neq g_{\mathbf{p}}^{yy,0}$  can induce an anisotropy in the total conductivity  $\sigma^{xx} \neq \sigma^{yy}$  even if the dispersion and, consequently, the quasiparticle velocity are symmetric. We see an example in the following flat band model.

### C. Flat band model

We apply our theory to a two-band model hosting a topological non-trivial flat lower and a dispersive upper band which was introduced in Ref. [55]. We show the band structure in Fig. 2. The complete Hamiltonian and the explicit form of the two bands  $E_{\mathbf{p}}^{\pm}$  are provided in the appendix. We use  $t$  as our unit of energy and set the lattice constant  $a = 1$ . We fix the chemical potential to the center of the lower band and analyze the longitudinal conductivity and its different contributions in the following. In the left figure of Fig. 3 we show the total longitudinal

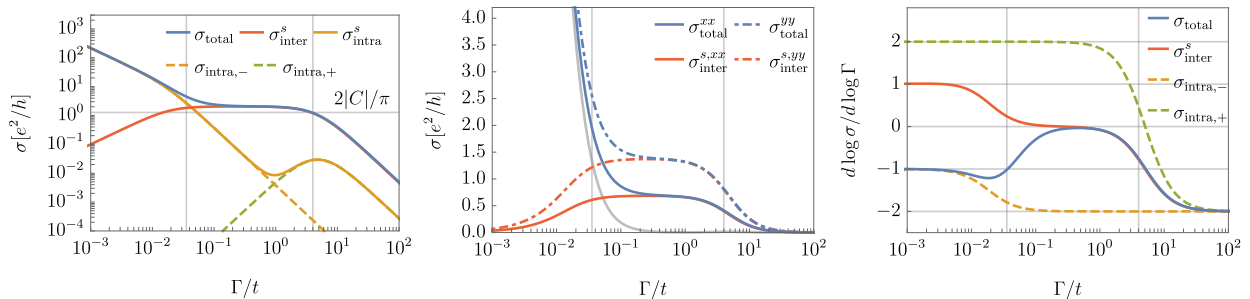


Figure 3. The longitudinal conductivity for the flat band model with chemical potential fixed to the center of the lower and (almost) flat band,  $\mu = (\mu_{\max}^{\min} + \mu_{\min}^{\max})/2 = -2.432t$ . *Left figure:* The total conductivity  $\sigma_{\text{total}}^{xx} + \sigma_{\text{total}}^{yy}$  (blue) with its intraband (orange) and geometric interband contribution (red) as a function of  $\Gamma/t$ . The conductivity is dominated by the geometric interband contribution, which is bounded from below (horizontal line) due to the finite Chern number  $|C| = 2$ , in an intermediate regime given by the band width of the flat band  $W_-/t = 0.036$  and the band gap  $\Delta/t = 4$  (vertical lines). At small  $\Gamma$  the conductivity is dominated by the intraband contribution of the (almost) flat band (dashed orange). *Middle figure:* The conductivity is different in  $x$  and  $y$  directions (solid and dash-dotted) due to the geometric interband contributions (red) in the intermediate regime (vertical lines). The intraband contribution (gray) is equal in both directions. *Right figure:* The scaling behavior of the different contributions. At low and large  $\Gamma$  the total conductivity and its contributions scale as expected [39]. In the intermediate regime we find a dissipationless regime.

conductivity  $\sigma_{\text{total}} = \sigma^{xx} + \sigma^{yy}$  (blue) calculated via (7) at zero temperature as a function of  $\Gamma/t$ . We clearly identify three different regimes with the crossover scales given by the band width of the flat band  $W_-/t = 0.036$  and the band gap  $\Delta/t = 4$ . For small  $\Gamma \lesssim W_-$  the conductivity is dominated by the intraband contribution (8) (orange) due to the small but finite quasiparticle velocities with maximal values  $v_{\max}^{x,-} = v_{\max}^{y,-} = 0.076t$  of the flat band (dashed orange). For an intermediate relaxation rate,  $W_- \lesssim \Gamma \lesssim \Delta$ , the quantum metric contribution (9) (red) is independent of  $\Gamma$  and bounded from below by the finite Chern number  $C_- = -2$  of the flat band according to (25) and (26), respectively. Above the threshold  $\Gamma_c \approx 0.134$  the total conductivity is dominated by the quantum metric contribution. For large  $\Gamma \gtrsim \Delta$  the total conductivity is strongly suppressed.

In the middle figure of Fig. 3 we show the longitudinal conductivity in  $x$  and  $y$  direction as function of  $\Gamma/t$ . The quasiparticle velocity is equal in both spatial directions,  $v_{\mathbf{p}}^{x,-} = v_{\mathbf{p}}^{y,-}$ , resulting in a direction-independent intraband contribution (gray). However, the quantum metric is different in  $x$  and  $y$  direction,  $g_{\mathbf{p}}^{xx,-} \neq g_{\mathbf{p}}^{yy,-}$ . We have

$$\bar{g}_{-}^{xx} \equiv \int \frac{d^2\mathbf{p}}{(2\pi)^2} g_{\mathbf{p}}^{xx,-} = \frac{K(-1/8)}{2\sqrt{2}\pi} \approx 0.17161, \quad (28)$$

$$\bar{g}_{-}^{yy} \equiv \int \frac{d^2\mathbf{p}}{(2\pi)^2} g_{\mathbf{p}}^{yy,-} = \frac{K(-1/8)}{\sqrt{2}\pi} \approx 0.34322, \quad (29)$$

where  $K(m) = \int_0^{\pi/2} 1(1 - m \sin^2 \theta)^{-1/2} d\theta$  is the complete elliptic integral of the first kind. We see that the mean quantum metric  $\bar{g}_{-}^{yy}$  in  $y$  direction is twice as large as the mean quantum metric  $\bar{g}_{-}^{xx}$  in  $x$  direction. According to (25) we obtain  $\sigma^{yy}/\sigma^{xx} = 2$  in the intermediate regime  $W_- \lesssim \Gamma \lesssim \Delta$  (blue) caused by the quantum metric contribution (red).

In the right figure of Fig. 3 we plot the logarithmic

derivative of the different conductivity contributions as a function of  $\Gamma/t$ . For  $\Gamma \ll W_-$  we have  $\sigma_{\text{intra,-}} \sim 1/\Gamma$  and  $\sigma_{\text{inter}}^s \sim \Gamma$  as expected for the clean limit behavior for a metal as discussed above. The intraband contribution of the upper band scales as  $\sigma_{\text{intra,+}} \sim \Gamma^2$  [39]. For  $\Gamma \gg \Delta$ , we have  $\sigma_{\text{intra,\pm}} \sim \sigma_{\text{inter}}^s \sim 1/\Gamma^2$  [39]. In the intermediate regime  $W_- \ll \Gamma \ll \Delta$ , we have  $\sigma_{\text{intra,-}} \sim 1/\Gamma^2$  and  $\sigma_{\text{inter}}^s \sim 1$  as expected by (23) and (24), respectively.

The general properties are robust against change in the parameters. We slightly modified the model to check the impact of a larger band width  $W_-$  and a broken symmetry in  $x$  and  $y$  direction,  $v_{\mathbf{p}}^{x,n} \neq v_{\mathbf{p}}^{y,n}$ . Consistent with our general arguments, larger  $W_-$  increases the intraband contribution  $\sigma_{\text{intra,-}}$  and reduces the regime where the quantum metric contribution dominates. A broken directional symmetry causes an anisotropy in the interband contributions, such that  $\sigma^{xx} \neq \sigma^{yy}$  also for  $\Gamma \lesssim W_-$ . Note that the ratio  $\sigma^{yy}/\sigma^{xx}$  is still different in the two regimes  $\Gamma \ll W_-$  and  $W_- \ll \Gamma \ll \Delta$  in general due to the different physical origin.

#### D. Rhombohedral trilayer graphene

We apply our theory to a realistic six-band low-energy model of the two-dimensional rhombohedral trilayer graphene in the regime of low carrier density where the fourfold flavor-symmetry in valley and spin is broken and only one flavor is occupied [11]. The full Hamiltonian and the parameters are summarized in the appendix. The material is highly tunable via an electrical displacement field, which introduces an energy gap  $\Delta_1$ . The band structure is shown in Fig. 2. Bands number 3 (orange) and 4 (blue) are almost flat within a momentum range of  $|\mathbf{p}|/a_0 \lesssim 0.05$ , where  $a_0$  is the lattice constant. In the following, we probe the longitudinal conductivity at the

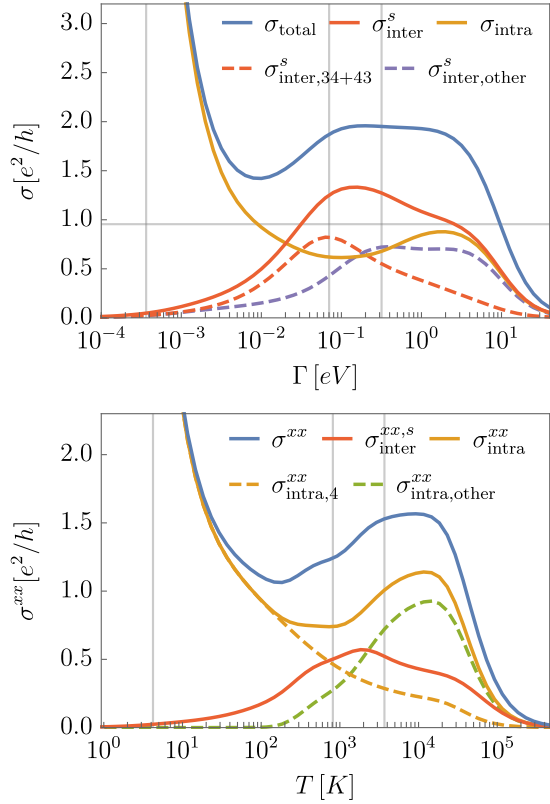


Figure 4. The contributions to the total longitudinal conductivity of rhombohedral trilayer graphene. *Upper figure:* The total conductivity (blue) and its intraband (orange) and geometric interband (red) contributions as a function of  $\Gamma$  for  $\mu = 1.05 \mu_{4,\min}$  and  $\Delta_1 = 40$  meV at  $T = 0$ . The main contribution to  $\sigma_{\text{intra}}^s$  at intermediate  $\Gamma$  are due to interband couplings of band 3 and 4 (red dashed) but all other 14 couplings contribute (purple dashed) significantly. *Lower figure:* The total (blue) contributions and its intraband (orange) and geometric interband (red) contributions as a function of temperature  $T$  for the same parameters with  $\Gamma = k_B T$ . At low  $T$  the intraband contribution is dominated by band 4 (orange dashed). At higher  $T$  the other bands (purple dashed) contribute significantly. The geometric contribution causes a conductivity minimum within the temperature range  $T \approx 50 \dots 400$  K.

lower edge  $\mu_{4,\min}$  of the nearly flat conduction band 4. The integration was performed on a square region up to a momentum cutoff  $\pi a_0 \gg 0.05 a_0$ .

In Fig. 4 (top panel) we show the obtained total conductivity  $\sigma_{\text{total}} = \sigma^{xx} + \sigma^{yy}$  (blue) and its quantum metric (red) and intraband (orange) contribution as a function of  $\Gamma$  at zero temperature. We fix  $\Delta_1 = 40$  meV and  $\mu = \mu_{4,\min} + 1.4$  meV. Although the band structure is more complicated than for the flat band model, which we discussed previously, we find similar characteristic regimes. For intermediate relaxation rates between  $\Gamma \approx 0.03 \dots 3$  eV we find a large geometric interband contribution exceeding the lower bound (26) due to the Berry charges totaling  $C_4 = 3/2$  near the band bottom of the fourth band. For small values of  $\Gamma$  the main part of the quantum metric

contribution is due to the interband coupling of the close bands 3 and 4, i.e.  $\sigma_{\text{inter}}^s \approx \sigma_{\text{inter},34}^s + \sigma_{\text{inter},43}^s$ . For larger  $\Gamma$  the quantum metric contribution of all other 28 interband couplings  $\sigma_{\text{inter},\text{other}}^s$  are required to exceed the lower bound. This might become important when using projections on a single band. Note that, in contrast to the flat band model discussed before, the intermediate regime cannot be easily connected to the characteristic energy scales of the system (vertical gray lines for the band width of the fourth band  $W_4$  and the gaps to the third and fifth band  $\Delta_{34}$  and  $\Delta_{45}$ , respectively). The main reason is based on the finite momentum range, in which the fourth band is flat: The relevant spectral weighting factors  $w_{\mathbf{p},\text{inter}}^{3n,s}(0)$  and  $w_{\mathbf{p},\text{inter}}^{n3,s}(0)$  with band index  $n \neq 3$  of the other five bands fulfill only approximately (24) for momenta  $\mathbf{p}/a_0 \lesssim 0.05$  and are strongly suppressed otherwise. Thus, the range of the momentum integration in (25) is restricted and do not capture the full quantum metric, which is maximal for  $0.03 \lesssim (g_{\mathbf{p}}^{xx,4} + g_{\mathbf{p}}^{yy,4})/a_0 \lesssim 0.12$ . The maximal value of  $\sigma_{\text{inter}}^s$  at  $\Gamma \approx 0.2$  eV is a subtle interplay between the spectral weighting factors and the quantum metric in (9). The upper scale is given by the momentum cutoff. At very low  $\Gamma \sim W_4 = 0.4$  meV of the order of the band width of the flat band  $W_4$ , the conductivity is dominated by the intraband contribution as expected due to the existence of a Fermi surface. Due to the upturn of the flat band at  $|\mathbf{p}|/a_0 \approx 0.05$  and the corresponding finite quasiparticle velocities, the interband contribution is nonzero over the full range of  $\Gamma$ , in particular, when  $\Gamma$  exceeds the gaps to band 3 and 5 with  $\Delta_{34} = 70$  meV and  $\Delta_{45} = 317$  meV. The upper scale is again given by the momentum cutoff.

The temperature dependence of the conductivity in RTG beyond 100K has not yet been investigated in detail, but the presence of flat bands and the emergence of superconducting phases at low temperatures suggests that the material offers a similar phenomenology to TBG. The latter has been shown to exhibit a very large linear-T resistivity, possibly making it a Planckian metal [17] in which the relaxation rate is close to a putative upper bound  $\mathcal{O}(k_B T)$ . Therefore, for the discussion of the temperature dependence and possible experimental signatures in RTG, we feel it is justified to assume the 'best case scenario' for our purposes, where  $\Gamma \sim k_B T$  with a coefficient close to 1. In the lower figure of Fig. 4 we show the conductivity  $\sigma^{xx}$  (blue) and its quantum metric (red) and intraband (orange) contributions as a function of temperature. We used the same parameters for  $\Delta_1$  and  $\mu$  as in the upper figure and assumed a relaxation rate of  $\Gamma = k_B T$ . Since rhombohedral trilayer graphene has a  $C_3$ -symmetry, it is  $\sigma^{xx} \neq \sigma^{yy}$ . However, the asymmetry is very small, with both conductivities differing by much less than one percent for a broad range of parameters. According to Eqs. (8) and (9) a finite temperature enters not only through the band broadening, but also via the Fermi-Dirac function in the spectral weights. Nevertheless, the characteristic behavior of the different contributions are qualitatively similar to the zero temperature case. In the low temperature regime,

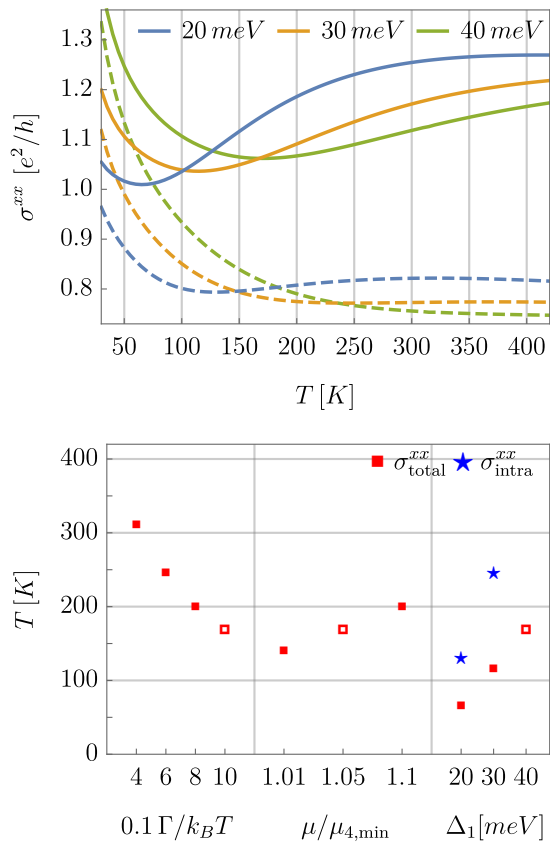


Figure 5. The quantum-metric induced conductivity minimum in trilayer graphene. *Upper figure:* The total (solid) and the intraband (dashed) conductivity as a function of temperature for different  $\Delta_1$  at fixed  $\mu = 1.05 \mu_{4,\min}$  and  $\Gamma = k_B T$ . *Lower figure:* The temperature of the minimal total (red filled and empty box) and intraband (blue star) conductivity for different parameters compared to  $\mu = 1.05 \mu_{4,\min}$ ,  $\Gamma = k_B T$ , and  $\Delta_1 = 40$  meV (empty box).

$T \sim W_4/k_B \approx 5$  K, the conductivity is mainly given by the intraband contribution, in particular, of the fourth band (orange and dashed), which can be understood by the scaling argument  $\sigma_{\text{intra}}^{xx} \sim 1/\Gamma \sim 1/T$ . At high temperature, especially beyond  $T \sim \Delta_{34}/k_B \approx 800$  K, the other bands contribute significantly (green and dashed). In an intermediate range the quantum metric contribution becomes crucial. We see that the temperature broadening by the Fermi function enhances the intraband contribution, whereas the quantum metric contribution is affected very little.

The conductivity  $\sigma^{xx}$  exhibits a minimum at approximately  $T_{\min} \approx 170$  K. The decomposition into its contributions shown in Fig. 4 reveals the origin of this minimum. It is caused by the decrease of the intraband contribution of the almost flat fourth band and the increase of the quantum metric contribution. It is important to notice that the thermal activation of the other bands leading to further intraband contributions is not sufficient to cause a minimum at such a low energy scale  $k_B T_{\min} \sim 15$  meV, which

is much smaller than the smallest gap  $\Delta_{34} = 70$  meV. The intraband contributions of the other bands lead to a second kink at much higher temperature. Thus, we have identified a minimum of the longitudinal conductivity due to virtual processes, i.e. effects of the quantum metric in rhombohedral trilayer graphene.

In Fig. 5 we discuss the stability and trends of the minimum for different parameter values. In the top panel we show  $\sigma^{xx}$  (solid) and the corresponding intraband contribution (dashed) for different  $\Delta_1$  at fixed  $\Gamma = k_B T$  and  $\mu/\mu_{4,\min} = 1.05$ , that is  $\mu - \mu_{4,\min} = 1.4, 0.9, 0.4$  meV for  $\Delta_1 = 40, 30, 20$  meV. We see a pronounced minimum for all three parameter sets. The comparison to the intraband contribution clearly shows that this minimum is caused by virtual processes captured by the quantum metric and not by thermal activation of intraband processes. Only a small minimum at significant higher temperature can be found for  $\Delta_1 = 20$  meV (blue) and  $\Delta_1 = 30$  meV (orange). We summarize the temperature of the conductivity minimum in the lower figure of Fig. 5 for these and further parameters of  $\Gamma/k_B T$ ,  $\mu/\mu_{4,\min}$ , and  $\Delta_1$ . The minimum found in the lower figure of Fig. 4 is taken as a reference (empty red box). We see that decreasing the temperature dependence of  $\Gamma$  shifts the minimum to higher temperature. We understand this shift by both an increase of the intraband and a decrease of the quantum metric contribution by the following argument: The conductivity minimum at temperature  $T_{\min}$  satisfies  $d\sigma^{xx}/dT = 0$ . Assuming the scaling  $\sigma_{\text{intra}}^{xx} \sim 1/ak_B T$  and  $\sigma_{\text{inter}}^{xx,s} \sim ak_B T$  leads to  $T_{\min} \sim 1/a$  with  $a = 0.4, 0.6, 0.8$ , and  $1.0$ . Note that the assumed scaling is only expected for small temperature. An increase of the chemical potential  $\mu/\mu_{4,\min} = 1.01, 1.05$ , and  $1.1$ , that is  $\mu - \mu_{4,\min} = 0.3, 1.4$ , and  $2.8$  meV, respectively, increases the Fermi velocity on the Fermi surface [cf. Fig. 2]. This increases the intraband contribution (8), whereas the quantum metric contribution remains unchanged. Thus, the minimum shifts to higher temperatures. Modifying  $\Delta_1$  decreases the gap between band 3 and 4, which increases the quantum metric. This and a decrease of the intraband contribution shifts the minimum to lower temperature. Whereas the full conductivity  $\sigma^{xx}$  exhibits a conductivity minimum for all considered parameters, the intraband contribution  $\sigma_{\text{intra}}^{xx}$  does not show any minimum in the reasonable temperature for most of the parameters.

We end with a discussion of the limitations of our approach. Since the formalism makes exclusive use of the band broadening parameter  $\Gamma$ , a legitimate concern is whether vertex corrections and extrinsic scattering due to impurities can qualitatively affect the results presented here. While both these effects can indeed become problematic in semimetals which necessarily have a small density of states and a large Fermi velocity [50,56], for a flat band dispersion it is the opposite, as it has a large density of states and a vanishing quasiparticle velocity. It therefore behaves like ordinary metals with a large Fermi surface, where the quantum lifetime and the transport lifetime are identical and impurities effects are weak.

We also limited the analysis to the non-interacting case. Upon introducing interactions, additional interband processes become possible which are mediated by these interactions. Since this introduces additional virtual transitions, we expect it to increase both the effective  $\Gamma$  and the effective  $g$ . As a result, it could be that the bound on resistivity is only weakly fulfilled. Since the bound is already only weakly fulfilled due to the finite residual Fermi velocity in RTG, it does not affect our main conclusions. A more serious complication is the possible presence of ordered states near charge neutrality. Experimentally, a correlated insulating state seems to emerge for carrier densities below  $n_e = 0.05 \cdot 10^{-12} \text{cm}^{-2}$ , corresponding to a chemical potential of  $1 - 2 \text{meV}$  above the band termination, which is comparable to the densities considered here. It is presently unclear whether such a state will also exist in samples of lower mobility.

### III. CONCLUSIONS

We systematically explored the role of the quantum metric for the electrical conductivity for various semimetallic

and metallic model systems, finding that it contributes at leading order both if the density of states vanishes at semimetallic band crossing points, but also when the density of states diverges in systems with quenched bandwidth and vanishing Fermi velocity. We reported an upper bound on the resistivity for flatband materials with nonzero Berry curvature and elucidated the range of validity and the limitations of this bound. As a platform to explore the resistivity bound, we suggested to employ rhombohedral trilayer graphene, and gave a detailed account of the various crossover scales which are expected in the system.

It is of timely relevance to explore how interactions will change the phenomenology reported here, in particular with respect to the quantum metric, a band structure parameter like the Berry curvature which is probably quite robust against interaction effects.

### ACKNOWLEDGMENTS

We are very grateful to Erez Berg, Laura Classen, Johannes Hofmann, and Elio König for valuable discussions.

### IV. APPENDIX

In this appendix, we state the tight-binding Hamiltonians which were used in the numerical calculations for Figs. 3-5 of the main text.

#### A. Flat band model

As a toy model for topological flat bands we employ a square bipartite lattice where one band is flattened by longer-ranged hopping [55]. It reads explicitly,

$$\begin{aligned} \lambda_{\mathbf{p}}/t = & -a \frac{1 - \sqrt{2}}{2} \left[ \cos(2(p_x + p_y)) + \cos(2(p_x - p_y)) \right] \mathbb{1} - \sqrt{2} \left[ \cos(p_x + p_y) - \cos(p_x - p_y) \right] \sigma_z \\ & - 2 \left[ \cos\left(p_y + (1 - b)\frac{\pi}{4}\right) \cos\left(p_y + b\frac{\pi}{4}\right) + \cos\left(p_x + (1 - b)\frac{\pi}{4}\right) \sin\left(p_y + b\frac{\pi}{4}\right) \right] \sigma_x \\ & + 2 \left[ \cos\left(p_x + (1 - b)\frac{\pi}{4}\right) \sin\left(p_y - b\frac{\pi}{4}\right) + \cos\left(p_y + (1 - b)\frac{\pi}{4}\right) \sin\left(p_y + b\frac{\pi}{4}\right) \right] \sigma_y. \end{aligned} \quad (30)$$

Here, the parameter  $a$  modifies the band width  $W_-$  of the flat band by maintaining the symmetry in  $x$  and  $y$  directions. The parameter  $b$  both broadens the band width as well as breaks this symmetry. In the main text and in the following, we set  $a = b = 1$ . The eigenvalues are

$$E_{\mathbf{p}}^{\pm} = -(1 - \sqrt{2}) \cos 2p_x \cos 2p_y \pm \sqrt{6 + 2 \cos 2p_x \cos 2p_y}. \quad (31)$$

Note that  $E^{\pm}(p_x, p_y) = E^{\pm}(p_y, p_x)$ . Furthermore, numerically we find for the energies where the bands terminate the values  $E_{\text{max}}^+/t = 3.243$ ,  $E_{\text{min}}^+/t = 1.586$ ,  $E_{\text{max}}^-/t = -2.414$  and  $E_{\text{min}}^-/t = -2.450$ . We place the chemical potential in the middle of the flat band, at  $\mu = (E_{\text{max}}^- + E_{\text{min}}^-)/2 = -2.432$ .

## B. Rhombohedral trilayer graphene

The six band model for trilayer graphene is adapted from [11]. It holds for each valley degree of freedom and both spin degrees of freedom, meaning that the total number of bands is 24. At low electron or hole density, the system spontaneously breaks the fourfold degenerate ground state symmetry and resides in a single flavor-polarized state. Using  $\pi_{\mathbf{p}} = \xi p_x + i p_y$  with  $\xi = \pm 1$  for the valley degree of freedom, it is (choosing  $\xi = 1$ ),

$$\lambda_{\mathbf{p}} = \begin{pmatrix} \Delta_1 + \Delta_2 + \delta & \gamma_2/2 & v_0\pi_{\mathbf{p}}^\dagger & v_4\pi_{\mathbf{p}}^\dagger & v_3\pi_{\mathbf{p}} & 0 \\ \gamma_2/2 & \Delta_2 - \Delta_1 + \delta & 0 & v_3\pi_{\mathbf{p}}^\dagger & v_4\pi_{\mathbf{p}} & v_0\pi_{\mathbf{p}} \\ v_0\pi_{\mathbf{p}} & 0 & \Delta_1 + \Delta_2 & \gamma_1 & v_4\pi_{\mathbf{p}}^\dagger & 0 \\ v_4\pi_{\mathbf{p}} & v_3\pi_{\mathbf{p}} & \gamma_1 & -2\Delta_2 & v_0\pi_{\mathbf{p}}^\dagger & v_4\pi_{\mathbf{p}}^\dagger \\ v_3\pi_{\mathbf{p}}^\dagger & v_4\pi_{\mathbf{p}}^\dagger & v_4\pi_{\mathbf{p}} & v_0\pi_{\mathbf{p}} & -2\Delta_2 & \gamma_1 \\ 0 & v_0\pi_{\mathbf{p}}^\dagger & 0 & v_4\pi_{\mathbf{p}} & \gamma_1 & \Delta_2 - \Delta_1 \end{pmatrix} \quad (32)$$

where we used the shorthand  $v_i = \sqrt{3}a_0\gamma_i/2$ . The parameters take the following values [11]:  $\gamma_0 = 3.1$  eV,  $\gamma_1 = 0.38$  eV,  $\gamma_2 = -0.015$  eV,  $\gamma_3 = -0.29$  eV,  $\gamma_4 = -0.141$  eV,  $\delta = -0.0105$  eV, and  $\Delta_2 = -0.0023$  eV.

- 
- [1] Yuan Cao, Valla Fatemi, Shiang Fang, Kenji Watanabe, Takashi Taniguchi, Efthimios Kaxiras, and Pablo Jarillo-Herrero, “Unconventional superconductivity in magic-angle graphene superlattices,” *Nature* **556**, 43–50 (2018), [arXiv:1803.02342 \[cond-mat.mes-hall\]](#).
- [2] Yuan Cao, Valla Fatemi, Ahmet Demir, Shiang Fang, Spencer L. Tomarken, Jason Y. Luo, Javier D. Sanchez-Yamagishi, Kenji Watanabe, Takashi Taniguchi, Efthimios Kaxiras, Ray C. Ashoori, and Pablo Jarillo-Herrero, “Correlated insulator behaviour at half-filling in magic-angle graphene superlattices,” *Nature* **556**, 80–84 (2018), [arXiv:1802.00553 \[cond-mat.mes-hall\]](#).
- [3] Xiaobo Lu, Petr Stepanov, Wei Yang, Ming Xie, Mohammed Ali Aamir, Ipsita Das, Carles Urgell, Kenji Watanabe, Takashi Taniguchi, Guangyu Zhang, Adrian Bachtold, Allan H. MacDonald, and Dmitri K. Efetov, “Superconductors, orbital magnets and correlated states in magic-angle bilayer graphene,” *Nature* **574**, 653–657 (2019), [arXiv:1903.06513 \[cond-mat.str-el\]](#).
- [4] Matthew Yankowitz, Shaowen Chen, Hryhoriy Polshyn, Yuxuan Zhang, K. Watanabe, T. Taniguchi, David Graf, Andrea F. Young, and Cory R. Dean, “Tuning superconductivity in twisted bilayer graphene,” *Science* **363**, 1059–1064 (2019), [arXiv:1808.07865 \[cond-mat.mes-hall\]](#).
- [5] Aaron L. Sharpe, Eli J. Fox, Arthur W. Barnard, Joe Finney, Kenji Watanabe, Takashi Taniguchi, M. A. Kastner, and David Goldhaber-Gordon, “Emergent ferromagnetism near three-quarters filling in twisted bilayer graphene,” *Science* **365**, 605–608 (2019), [arXiv:1901.03520 \[cond-mat.mes-hall\]](#).
- [6] U. Zondiner, A. Rozen, D. Rodan-Legrain, Y. Cao, R. Queiroz, T. Taniguchi, K. Watanabe, Y. Oreg, F. von Oppen, Ady Stern, E. Berg, P. Jarillo-Herrero, and S. Ilani, “Cascade of phase transitions and Dirac revivals in magic-angle graphene,” *Nature* **582**, 203–208 (2020), [arXiv:1912.06150 \[cond-mat.mes-hall\]](#).
- [7] Xiaomeng Liu, Zeyu Hao, Eslam Khalaf, Jong Yeon Lee, Yuval Ronen, Hyobin Yoo, Danial Haei Najafabadi, Kenji Watanabe, Takashi Taniguchi, Ashvin Vishwanath, *et al.*, “Tunable spin-polarized correlated states in twisted double bilayer graphene,” *Nature* **583**, 221–225 (2020).
- [8] Guorui Chen, Aaron L. Sharpe, Eli J. Fox, Ya-Hui Zhang, Shaoxin Wang, Lili Jiang, Bosai Lyu, Hongyuan Li, Kenji Watanabe, Takashi Taniguchi, Zhiwen Shi, T. Senthil, David Goldhaber-Gordon, Yuanbo Zhang, and Feng Wang, “Tunable correlated Chern insulator and ferromagnetism in a moiré superlattice,” *Nature* **579**, 56–61 (2020), [arXiv:1905.06535 \[cond-mat.mes-hall\]](#).
- [9] Jeong Min Park, Yuan Cao, Kenji Watanabe, Takashi Taniguchi, and Pablo Jarillo-Herrero, “Tunable strongly coupled superconductivity in magic-angle twisted trilayer graphene,” *Nature* **590**, 249–255 (2021).
- [10] Zeyu Hao, AM Zimmerman, Patrick Ledwith, Eslam Khalaf, Danial Haie Najafabadi, Kenji Watanabe, Takashi Taniguchi, Ashvin Vishwanath, and Philip Kim, “Electric field-tunable superconductivity in alternating-twist magic-angle trilayer graphene,” *Science* **371**, 1133–1138 (2021).
- [11] Haoxin Zhou, Tian Xie, Areg Ghazaryan, Tobias Holder, James R. Ehrets, Eric M. Spanton, Takashi Taniguchi, Kenji Watanabe, Erez Berg, Maksym Serbyn, and Andrea F. Young, “Half and quarter metals in rhombohedral trilayer graphene,” *Nature* **598**, [arXiv:2104.00653 \(2021\)](#), [arXiv:2104.00653 \[cond-mat.mes-hall\]](#).
- [12] Haoxin Zhou, Tian Xie, Takashi Taniguchi, Kenji Watanabe, and Andrea F. Young, “Superconductivity in rhombohedral trilayer graphene,” [arXiv](#), [arXiv:2106.07640 \(2021\)](#), [arXiv:2106.07640 \[cond-mat.mes-hall\]](#).
- [13] Lei Wang, En-Min Shih, Augusto Ghiotto, Lede Xian, Daniel A. Rhodes, Cheng Tan, Martin Claassen, Dante M. Kennes, Yusong Bai, Bumho Kim, Kenji Watanabe, Takashi Taniguchi, Xiaoyang Zhu, James Hone, Angel Rubio, Abhay Pasupathy, and Cory R. Dean, “Correlated electronic phases in twisted bilayer transition metal

- dichalcogenides,” *Nat. Mater.* **19**, arXiv:1910.12147 (2020), arXiv:1910.12147 [cond-mat.mes-hall].
- [14] Zhiming Zhang, Yimeng Wang, Kenji Watanabe, Takashi Taniguchi, Keiji Ueno, Emanuel Tutuc, and Brian J. LeRoy, “Flat bands in twisted bilayer transition metal dichalcogenides,” *Nat. Phys.* **16**, arXiv:1910.13068 (2020), arXiv:1910.13068 [cond-mat.str-el].
- [15] Hryhoriy Polshyn, Matthew Yankowitz, Shaowen Chen, Yuxuan Zhang, K. Watanabe, T. Taniguchi, Cory R. Dean, and Andrea F. Young, “Large linear-in-temperature resistivity in twisted bilayer graphene,” *Nat. Phys.* **15**, 1011–1016 (2019).
- [16] Aavishkar A. Patel and Subir Sachdev, “Theory of a Planckian Metal,” *Phys. Rev. Lett.* **123**, 066601 (2019), arXiv:1906.03265 [cond-mat.str-el].
- [17] Yuan Cao, Debanjan Chowdhury, Daniel Rodan-Legrain, Oriol Rubies-Bigorda, Kenji Watanabe, Takashi Taniguchi, T. Senthil, and Pablo Jarillo-Herrero, “Strange Metal in Magic-Angle Graphene with near Planckian Dissipation,” *Phys. Rev. Lett.* **124**, 076801 (2020), arXiv:1901.03710 [cond-mat.str-el].
- [18] Augusto Ghiotto, En-Min Shih, Giancarlo S. S. G. Pereira, Daniel A. Rhodes, Bumho Kim, Jiawei Zang, Andrew J. Millis, Kenji Watanabe, Takashi Taniguchi, James C. Hone, Lei Wang, Cory R. Dean, and Abhay N. Pasupathy, “Quantum criticality in twisted transition metal dichalcogenides,” *Nature* **597**, 345–349 (2021), arXiv:2103.09796 [cond-mat.mes-hall].
- [19] Rafi Bistritzer and Allan H. MacDonald, “Moiré bands in twisted double-layer graphene,” *PNAS* **108**, 12233–12237 (2011), arXiv:1009.4203 [cond-mat.mes-hall].
- [20] J. M. B. L. Santos, N. M. R. Peres, and A. H. Castro Neto, “Continuum model of the twisted graphene bilayer,” *Phys. Rev. B* **86**, 155449 (2012), arXiv:1202.1088 [cond-mat.mtrl-sci].
- [21] Mikito Koshino and Edward McCann, “Trigonal warping and berry’s phase  $n\pi$  in ABC-stacked multilayer graphene,” *Phys. Rev. B* **80**, 165409 (2009).
- [22] Fan Zhang, Bhagawan Sahu, Hongki Min, and A. H. MacDonald, “Band structure of ABC-stacked graphene trilayers,” *Phys. Rev. B* **82**, 035409 (2010).
- [23] Mikito Koshino, “Interlayer screening effect in graphene multilayers with ABA and ABC stacking,” *Phys. Rev. B* **81**, 125304 (2010).
- [24] Kin Fai Mak, Jie Shan, and Tony F. Heinz, “Electronic structure of few-layer graphene: Experimental demonstration of strong dependence on stacking sequence,” *Phys. Rev. Lett.* **104**, 176404 (2010).
- [25] David R. Nelson and J. M. Kosterlitz, “Universal Jump in the Superfluid Density of Two-Dimensional Superfluids,” *Phys. Rev. Lett.* **39**, 1201–1205 (1977).
- [26] Sebastiano Peotta and Päivi Törmä, “Superfluidity in topologically nontrivial flat bands,” *Nat. Commun.* **6**, 8944 (2015), arXiv:1506.02815 [cond-mat.supr-con].
- [27] Long Liang, Tuomas I. Vanhala, Sebastiano Peotta, Topi Siro, Ari Harju, and Päivi Törmä, “Band geometry, Berry curvature, and superfluid weight,” *Phys. Rev. B* **95**, 024515 (2017), arXiv:1610.01803 [cond-mat.supr-con].
- [28] Xiang Hu, Timo Hyart, Dmitry I. Pikulin, and Enrico Rossi, “Geometric and Conventional Contribution to the Superfluid Weight in Twisted Bilayer Graphene,” *Phys. Rev. Lett.* **123**, 237002 (2019), arXiv:1906.07152 [cond-mat.supr-con].
- [29] A. Julku, T. J. Peltonen, L. Liang, T. T. Heikkilä, and P. Törmä, “Superfluid weight and Berezinskii-Kosterlitz-Thouless transition temperature of twisted bilayer graphene,” *Phys. Rev. B* **101**, 060505 (2020), arXiv:1906.06313 [cond-mat.mes-hall].
- [30] Nicola Marzari and David Vanderbilt, “Maximally localized generalized Wannier functions for composite energy bands,” *Phys. Rev. B* **56**, 12847–12865 (1997), arXiv:cond-mat/9707145 [cond-mat.mtrl-sci].
- [31] Nicola Marzari, Arash A. Mostofi, Jonathan R. Yates, Ivo Souza, and David Vanderbilt, “Maximally localized Wannier functions: Theory and applications,” *Rev. Mod. Phys.* **84**, 1419–1475 (2012), arXiv:1112.5411 [cond-mat.mtrl-sci].
- [32] R. Resta, “The insulating state of matter: a geometrical theory,” *Euro. Phys. J. B* **79**, 121–137 (2011), arXiv:1012.5776 [cond-mat.mtrl-sci].
- [33] Yang Gao, Shengyuan A. Yang, and Qian Niu, “Geometrical effects in orbital magnetic susceptibility,” *Phys. Rev. B* **91**, 214405 (2015), arXiv:1411.0324 [cond-mat.mes-hall].
- [34] Michael Kolodrubetz, Dries Sels, Pankaj Mehta, and Anatoli Polkovnikov, “Geometry and non-adiabatic response in quantum and classical systems,” *Phys. Rep.* **697**, 1–87 (2017), arXiv:1602.01062 [cond-mat.quant-gas].
- [35] Yang Gao and Di Xiao, “Nonreciprocal Directional Dichroism Induced by the Quantum Metric Dipole,” *Phys. Rev. Lett.* **122**, 227402 (2019), arXiv:1810.02728 [cond-mat.mes-hall].
- [36] Tobias Holder, Daniel Kaplan, and Binghai Yan, “Consequences of time-reversal-symmetry breaking in the light-matter interaction: Berry curvature, quantum metric, and diabatic motion,” *Phys. Rev. Research* **2**, 033100 (2020), arXiv:1911.05667 [cond-mat.mes-hall].
- [37] Junyeong Ahn, Guang-Yu Guo, Naoto Nagaosa, and Ashvin Vishwanath, “Riemannian Geometry of Resonant Optical Responses,” arXiv, arXiv:2103.01241 (2021), arXiv:2103.01241 [cond-mat.mes-hall].
- [38] J. P. Provost and G. Vallee, “Riemannian structure on manifolds of quantum states,” *Commun. Math. Phys.* **76**, 289–301 (1980).
- [39] Johannes Mitscherling, “Longitudinal and anomalous Hall conductivity of a general two-band model,” *Phys. Rev. B* **102**, 165151 (2020), arXiv:2008.11218 [cond-mat.str-el].
- [40] Tobias Holder and Binghai Yan, “Electrons flow like falling cats,” to be published (2021).
- [41] A. H. Castro Neto, F. Guinea, N. M. R. Peres, K. S. Novoselov, and A. K. Geim, “The electronic properties of graphene,” *Rev. Mod. Phys.* **81**, 109–162 (2009), arXiv:0709.1163.
- [42] B. Roy and S. Das Sarma, “Diffusive quantum criticality in three-dimensional disordered Dirac semimetals,” *Phys. Rev. B* **90**, 241112 (2014), arXiv:1407.7026 [cond-mat.dis-nn].
- [43] Tomoki Ozawa and Bruno Mera, “Relations between topology and the quantum metric for Chern insulators,” *Phys. Rev. B* **104**, 045103 (2021), arXiv:2103.11582 [cond-mat.mes-hall].
- [44] Shunji Matsuura and Shinsei Ryu, “Momentum space metric, nonlocal operator, and topological insulators,” *Phys. Rev. B* **82**, 245113 (2010), arXiv:1007.2200 [cond-mat.mes-hall].
- [45] S. A. Hartnoll, “Theory of universal incoherent metallic transport,” *Nat. Phys.* **11**, 54–61 (2015), arXiv:1405.3651 [cond-mat.str-el].

- [46] A. Lucas and S. A. Hartnoll, “Resistivity bound for hydrodynamic bad metals,” *PNAS* **114**, 11344–11349 (2017), arXiv:1704.07384 [cond-mat.str-el].
- [47] T. Hartman, S. A. Hartnoll, and R. Mahajan, “Upper Bound on Diffusivity,” *Phys. Rev. Lett.* **119**, 141601 (2017).
- [48] Johannes Mitscherling and Walter Metzner, “Longitudinal conductivity and Hall coefficient in two-dimensional metals with spiral magnetic order,” *Phys. Rev. B* **98**, 195126 (2018), arXiv:1807.10252 [cond-mat.str-el].
- [49] N. W. Ashcroft and N. D. Mermin, *Solid State Physics* (Holt-Saunders, 1976).
- [50] Naoto Nagaosa, Jairo Sinova, Shigeki Onoda, A. H. MacDonald, and N. P. Ong, “Anomalous Hall effect,” *Rev. Mod. Phys.* **82**, 1539–1592 (2010), arXiv:0904.4154 [cond-mat.mes-hall].
- [51] D. Xiao, M.-C. Chang, and Q. Niu, “Berry phase effects on electronic properties,” *Rev. Mod. Phys.* **82**, 1959–2007 (2010), arXiv:0907.2021 [cond-mat.mes-hall].
- [52] Pietro M. Bonetti, Johannes Mitscherling, Demetrio Vilardi, and Walter Metzner, “Charge carrier drop at the onset of pseudogap behavior in the two-dimensional Hubbard model,” *Phys. Rev. B* **101**, 165142 (2020), arXiv:2002.02786 [cond-mat.str-el].
- [53] Zhiqiang Wang, Gaurav Chaudhary, Qijin Chen, and K. Levin, “Quantum geometric contributions to the BKT transition: Beyond mean field theory,” *Phys. Rev. B* **102**, 184504 (2020), arXiv:2007.15028 [cond-mat.supr-con].
- [54] Rahul Roy, “Band geometry of fractional topological insulators,” *Phys. Rev. B* **90**, 165139 (2014).
- [55] Johannes S. Hofmann, Erez Berg, and Debanjan Chowdhury, “Superconductivity, pseudogap, and phase separation in topological flat bands,” *Phys. Rev. B* **102**, 201112 (2020), arXiv:1912.08848 [cond-mat.str-el].
- [56] N. A. Sinitsyn, A. H. MacDonald, T. Jungwirth, V. K. Dugaev, and Jairo Sinova, “Anomalous Hall effect in a two-dimensional Dirac band: The link between the Kubo-Streda formula and the semiclassical Boltzmann equation approach,” *Phys. Rev. B* **75**, 045315 (2007), arXiv:cond-mat/0608682 [cond-mat.mes-hall].